Craig-Gordon model validation using stable isotope ratios in water vapor over the Southern Ocean

Shaakir Shabir Dar[1], Prosenjit Ghosh[1,2], Ankit Swaraj[2], and Anil Kumar[3]

[1]Centre for Earth Sciences, Indian Institute of Science, Bengaluru, 560012, Karnataka, India.
[2]Divecha Centre for Climate Change, Indian Institute of Science, Bengaluru, 560012, Karnataka, India.
[3]National Centre for Polar and Ocean Research, Vaso-da-Gama, 403804, Goa, India.

Correspondence: Prosenjit Ghosh (pghosh@iisc.ac.in)

Abstract. The stable isotopic composition of water vapor over the ocean is governed by the isotopic composition of surface water, ambient vapor isotopic composition, exchange and mixing processes at the water-air interface as well as the local meteorological conditions. These parameters form inputs to the Craig-Gordon models, used for predicting the isotopic composition of vapor produced from the surface water due to the evaporation process. In this study we present water vapor, surface water isotope ratios and meteorological parameters across latitudinal transects in the Southern Ocean ($27.38°$S to $69.34°$S and $21.98°$S to $66.8°$) during two austral summers. The performance of Traditional Craig-Gordon (TCG) (Craig and Gordon, 1965) and the Unified Craig-Gordon (UCG) (Gonfiantini et al., 2018) models is evaluated to predict the isotopic composition of evaporated water vapor flux in the diverse oceanic settings. The models are run for the molecular diffusivity ratios suggested by (Merlivat, 1978) (MJ), (Cappa et al., 2003) (CD) and (Pfahl and Wernli, 2009) (PW) and different turbulent indices (x) i.e. fractional contribution of molecular vs turbulent diffusion. It is found that the $UCG^{MJ}_{x=0.8}, UCG^{CD}_{x=0.6}, TCG^{MJ}_{x=0.6}$ and $TCG^{CD}_{x=0.7}$ models predicted the isotopic composition that best matches with the observations. The relative contribution from locally generated and advected moisture is calculated at the water vapor sampling points, along the latitudinal transects, assigning the representative end member isotopic compositions and by solving the two-component mixing model. The results suggest varying contribution of advected westerly component with an increasing trend up to 65°S. Beyond 65°S, the proportion of Antarctic moisture was found to be prominent and increasing linearly towards the coast.

1 Introduction

The knowledge of factors governing the evaporation of water from the oceans is an essential part of our understanding of the hydrological cycle. The oceans regulate the climate of the earth through heat and moisture transport (Chahine, 1992). Nearly $\approx 97\%$ of the water of earth is in the oceans as saline while the residual $\approx 3\%$ is fresh water stored in groundwater, glaciers and lakes, or flowing as rivers and streams (Korzoun and Sokolov, 1978). Evaporation of ocean water generates vapour and forms the initial reservoir for circulation in the hydrological cycle. A fraction of this vapor, only $\approx 10\%$ of it is transported inland to generate precipitation, while rest of the moisture precipitates over the ocean during its transit (Oki and Kanae, 2006; Shiklomanov, 1998).

Measurements of the isotope composition of water in the various reservoirs of the hydrological cycle operating over the oceans is useful to infer information about the origin of water masses and understanding the formation mechanisms, transport pathways and finally the precipitation processes (Craig, 1961; Dansgaard, 1964; Yoshimura, 2015; Gat, 1996; Araguás-Araguás et al., 2000; Noone and Sturm, 2010; Gat et al., 2003; Benetti et al., 2014; Galewsky et al., 2016). Comparatively large volume of data exists over land to understand the terrestrial hydrological cycle, through the Global Network in Precipitation (GNIP) initiative of the International Atomic Energy Agency (IAEA). However, only a handful records on the spatial and temporal variability of precipitation and vapor isotopic composition over the oceans is available for any assessment (e.g. the Indian Ocean and the Southern Ocean (Uemura et al., 2008; Rahul et al., 2018; Prasanna et al., 2018), the Atlantic Ocean (Benetti et al., 2017b, a, 2015) and Mediterranean Sea (Gat et al., 2003)). Hence further effort is needed to enhance the spatial and temporal sampling coverage over the oceans.

The isotopic composition of vapor on top of a water body is governed by the factors: i) Thermodynamic equilibrium process for phase transformation at a particular temperature ii) Kinetic or non-equilibrium processes where role of relative humidity and wind is significant and iii) Large-scale transport and mixing: due to the movement of air parcels laterally and vertically. Craig and Gordon (1965) initially proposed a two-layer model to simulate the isotopic composition of evaporated (referred to as the Traditional Craig-Gordon model). Recently, Gonfiantini et al. (2018) put forward a modified version referred to as the Unified Craig-Gordon Model. Both of these models incorporate the equilibrium and kinetic processes to simulate the isotopic composition of evaporated moisture. However, in order to get a realistic picture of the hydrological cycle over the ocean, the horizontal transport/advective mixing is important and should be incorporated.

In this paper we present stable isotope ratios in water vapor and ocean surface water from different locations covering varied oceanic settings; i.e. tropical, subtropical and polar latitudes, with a large range in the sea surface temperature, relative humidity and wind speed. While the role of temperature dependent equilibrium fractionation is well understood, the role of kinetic processes is under debate and requires further scrutiny. The performance of these Craig-Gordon evaporation models to simulate the isotopic composition of evaporation flux is evaluated along the sampling transect for different molecular diffusivity ratios and different fractions of molecular vs turbulent diffusion. The models and the conditions that best match with the observations are identified, which are then used to calculate the local evaporation flux. This as done in the context of estimating the contribution of advected vs in-situ derived vapor along the sampling transect assuming a complete mixing of the advected and the locally generated vapor in the sampled water vapor in our study.

2 Methods

2.1 Sampling, isotopic analysis and meteorological parameters

The samples (water vapor, and surface water) for this study were collected along the stretch from Mauritius to Prydz Bay (24°S to 69°S and 57°E to 76°E) during two successive austral summers (January 2017 (SOE-IX) and December 2017 to January 2018 (SOE-X)) onboard the ocean research vessel SA Agulhas. The water vapor sampling inlet was set at ≈ 15m above the sea level. An aggregate of 71 water vapor samples were collected during the two expeditions. Fig. 1 shows the water vapor sampling

locations. Alongside water vapor, 49 surface water samples were also collected. The details about the sampling procedures for collection of water vapor and surface water samples are given in the supplementary document. All these subjected to isotopic analysis using Finnigan Gasbench peripheral connected with an isotope ratio mass spectrometer (ThermoScientific MAT 253)

60 (details are provided in the supplementary document). The isotope ratios are expressed in ‰ using the standard δ notation relative to Vienna Standard Mean Ocean Water (VSMOW).

Along with water samples, relative humidity (h), wind speed (ws), air temperature (Ta), sea surface temperature (sst), and atmospheric pressure (P) was recorded continuously during the expedition. Fig. 2 shows the latitudinal variation of these meteorological parameters. A wide range of these physical conditions are encountered since the sampling encompasses a large

65 latitudinal transect.

2.2 Backward air-mass trajectories

In order to reconstruct the vertical profile of the atmospheric moisture transport along the sampling transect, backward air mass trajectories were generated using the Hybrid Single Particle Lagrangian Integrated Trajectory (HYSPLIT) model (Draxler and Hess, 1998; Stein et al., 2015) of NOAA-NCEP/NCAR forced with the Reanalysis data (Kanamitsu et al., 2002). HYSPLIT

70 is a computational model hybrid between Lagrangian and Eulerian methods which generates the paths traversed by the air parcels and calculates meteorological variables such as temperature, relative humidity, specific humidity, rainfall, pressure etc. along the route. Back trajectories for 3 days are extracted since the average residence time of atmospheric moisture over the oceans is $\approx$3 days Trenberth (1998); Van Der Ent and Tuinenburg (2017). Figure 3 shows the back trajectories for the water vapor sampling locations. The sampling locations can be broadly categorized into zones which are defined by different wind

75 patterns (i.e. velocity and the moisture carrying capacity). Westerlies and polar easterlies were identified based these 72 hour back-trajectories constructed at three different heights above the ocean surface. During the SOE X expedition, the change in trajectories to westerlies was at $\approx$31°S. At $\approx$63°S, change from westerlies to polar easterlies is seen. For SOE IX the transition from the westerlies to easterlies and then to polar westerlies was documented at the $\approx$33°S and $\approx$64°S latitudes respectively.

2.3 The Craig-Gordon Models

80 Craig-Gordon in 1965 (CG) Craig and Gordon (1965) proposed the first theoretical model to explain the isotopic composition of water vapor during the evaporation process. The isotopic composition of vapor generated on top of the ocean water depends on the isotopic composition of the surface oceanic water, the isotopic composition of water vapor in the ambient atmosphere along with the relative humidity at the site of sample collection. The interplay of equilibrium and kinetic fractionation between these phases governs the final isotopic composition in the water vapour and liquid. The equilibrium fractionation between ocean

85 water and vapor is controlled by the sea surface temperature (sst). In comparison, relative humidity and wind speed control the the kinetic fractionation through the combination of processes which include both molecular and turbulent diffusion. Molecular diffusion leads to isotopic fractionation between liquid and vapor whereas the turbulent diffusion is non-fractionating. To estimate the isotopic composition of water vapor CG model invokes two-layers; a laminar layer above the air-water interface where the transport process is active via molecular diffusion and a turbulent layer above the laminar layer in which the molecu-

3

lar transfer is predominantly by the action of turbulent diffusion. Assuming there is no divergence/convergence of air mass over the oceanic atmosphere, the isotopic ratio of the evaporation flux is given as Craig and Gordon (1965) referred to as Traditional Craig-Gordon Model (TCG):

$$R_{ev} = \alpha_k . \frac{R_L . \alpha_{eq} - h.R_A}{1-h} \tag{1}$$

Where R_L, R_A, h, α_k and α_{eq} are respectively, the isotopic composition of the liquid water, the isotopic composition environmental atmospheric moisture, relative humidity, the kinetic and the equilibrium fractionation factors. The TCG models in this form and with modifications have been used in diverse applications numerous studies studies. Above the ocean one can assume that a steady state is achieved in which the isotopic composition of vapor removed from the system has the same composition as atmospheric vapor (Merlivat, 1978). This is the global closure assumption, i.e,

$$R_A = R_{ev} \tag{2}$$

the global closure assumption (Eq. 2), is substituted in Eq (1) to give;

$$R_{ev} = \alpha_k . \frac{R_L . \alpha_{eq} - h.R_{ev}}{1-h} \tag{3}$$

$$R_{ev}(1-h) = \alpha_k . [R_L . \alpha_{eq} - h.R_{ev}] \tag{4}$$

$$R_{ev}(1-h) + \alpha_k h.R_{ev} = \alpha_k . R_L . \alpha_{eq} \tag{5}$$

$$R_{ev}[(1-h) + \alpha_k . h] = \alpha_k . R_L . \alpha_{eq} \tag{6}$$

$$R_{ev} = \frac{\alpha_{eq} \alpha_k R_L}{(1-h) + \alpha_k . h} \tag{7}$$

Recently, Gonfiantini et al. (2018) proposed a modified version of the model, termed as Unified Craig-Gordon (UCG) model in which the parameters controlling the isotopic composition of the evaporation flux are considered simultaneously. From Gonfiantini et al. (2018), the net evaporation rate of liquid water (E) is the difference between the vaporization rate, ψ_{vap}, and the atmospheric vapor capture rate (i.e; condensation) by the liquid water, ψ_{cap}.

$$E = \psi_{vap} - \psi_{cap} = (\gamma - h)\psi_{cap}^o \tag{8}$$

Where the ψ_{cap}^o is the vaporization rate of pure water, h is the relative humidity and γ is the thermodynamic activity coefficient of evaporating water which is <1 for the saline solutions and 1 for the pure water or dilute solutions.

From eq. (8), We can write;

$$R_{ev}(\gamma - h)\Psi_{vap}^o = R_{esc}\gamma\Psi_{vap}^o - R_{cap}h\Psi_{vap}^o \tag{9}$$

$$R_{ev}(\gamma - h)\Psi_{vap}^o = \frac{R_L}{\alpha_{eq}\alpha_{diff}^x}\gamma\Psi_{vap}^o - \frac{R_A}{\alpha_{diff}^x}h\Psi_{vap}^o \tag{10}$$

$$R_{ev} = \frac{\frac{R_L}{\alpha_{eq}\alpha_{diff}^x}\gamma - \frac{R_A}{\alpha_{diff}^x}h}{\gamma - h} \tag{11}$$

Where R_L, R_{esc}, R_{cap} and R_A are, respectively the isotopic composition of the liquid water, isotopic composition of vapor escaping to the saturated layer above which is in thermodynamic equilibrium with water, isotopic composition of environmental atmospheric moisture captured by the equilibrium layer and the isotopic composition environmental atmospheric moisture. R_L, R_{esc}, R_{cap} and R_A are defined as in Gonfiantini et al. (2018). α_{eq} is the isotopic fractionation factor between the liquid water and the vapor in the equilibrium layer. α_{diff} is the isotopic fractionation factor for diffusion in air affecting the vapor escaping from the equilibrium layer and the environmental vapor entering the equilibrium layer; x is the turbulent index of atmosphere. Introducing the global closure assumption, Eq. (2) in (11) gives;

$$R_{ev} = \frac{\frac{R_L}{\alpha_{eq}\alpha_{diff}^x}\gamma - \frac{R_{ev}}{\alpha_{diff}^x}h}{\gamma - h} \tag{12}$$

$$R_{ev}(\gamma - h) = \frac{R_L}{\alpha_{eq}\alpha_{diff}^x}\gamma - \frac{R_{ev}}{\alpha_{diff}^x}h \tag{13}$$

$$R_{ev}(\gamma - h) + \frac{R_{ev}}{\alpha_{diff}^x}h = \frac{R_L}{\alpha_{eq}\alpha_{diff}^x}\gamma \tag{14}$$

$$R_{ev}[(\gamma - h) + \frac{h}{\alpha_{diff}^x}] = \frac{R_L}{\alpha_{eq}\alpha_{diff}^x}\gamma \tag{15}$$

$$R_{ev}[\frac{(\gamma - h)\alpha_{diff}^x + h}{\alpha_{diff}^x}] = \frac{R_L}{\alpha_{eq}\alpha_{diff}^x}\gamma \tag{16}$$

$$R_{ev} = \frac{R_L}{\alpha_{eq}\alpha_{diff}^x}\gamma[\frac{\alpha_{diff}^x}{(\gamma - h)\alpha_{diff}^x + h}] \tag{17}$$

$$R_{ev} = \frac{R_L \gamma}{\alpha_{eq}[\alpha_{diff}^x(\gamma - h) + h]} \tag{18}$$

The temperature dependent equilibrium fractionation factor is calculated using the formulation given by (Horita and Wesolowski, 1994). The kinetic factor takes into account diffusion in air affecting the vapor escaping from the equilibrium layer and is controlled by α_{diff}, which is the molecular diffusivity of the different isotopologues of water. Molecular diffusivities ($H_2^{18}O/H_2^{16}O$, $H^2H^{16}O/H_2^{16}O$) data are taken from three previous studies Merlivat (1978) (1.0285, 1.0251), Cappa et al. (2003) (1.0318, 1.0164) and Pfahl and Wernli (2009) (1.0076, 1.0039) referred to as MJ, CD and PW respectively. x is the turbulence index of atmosphere. When x = 1 the vapor escapes solely by molecular diffusion and for x = 0 the vapor escapes only due to turbulent diffusion.

3 Results

3.1 Isotopic measurements along the transect

$\delta^{18}O$ of surface water was > 0 ‰ until $\approx$ 40°S latitude. A transition to lighter isotopic composition was observed beyond $\approx$ 45°S latitude with a drop documented in the surface water isotopic values on approaching the coastal Antarctic regions. Figure 4a shows the latitudinal variation of $\delta^{18}O_{sw}$, plotted along with salinity values measured along the transect. In addition, the $\delta^{18}O$ of ocean surface water extracted from the Global Sea Water 18O Database (SWD) (Schmidt et al., 1999) are also plotted. There is a mismatch between the observed depleted isotopic values near coastal Antarctica with SWD values. The SWD is a surface interpolated dataset based on point observations in the global ocean. This is probably one of the major causes of the difference, the others being the season or the month of sample collection.

The $\delta^{18}O_{wv}$ and δ^2H_{wv} in water vapor samples showed a consistent trend across latitude for both the expeditions. The $\delta^{18}O_{wv}$ (δ^2H_{wv}) of water vapor varies from -10.9‰ (-80.8‰) to -27.5‰(-221.4‰) respectively. The vapor isotopic composition is seen to be gradually decreasing with lighter isotopic values at higher latitudes. A steady drop was noted from $\approx$30°S to $\approx$65°S and a sharp change in the gradient was registered at $\approx$65°S. Extreme lighter values were recorded on approaching $\approx$65°S are attributed to factors like low temperature and the mixing of lighter vapor from continental Antarctica (Uemura et al., 2008). There are deviations from this general trend with heavier isotopic composition observed at the higher latitudes or vice versa. These variations can be accounted, by taking into consideration the source and the path of air masses. The lighter (heavier) values of vapor isotopic composition can be traced to the source being lower (higher) latitudes.

Deuterium excess (d-excess or dxs), defined as $d - excess = \delta^2H - 8 \times \delta^{18}O$, is a second order isotope parameter which is a measure of kinetic fractionation during evaporation (Dansgaard, 1964). d-excess in the water vapor correlates with meteorological parameters at the ocean surface such as relative humidity, sea surface temperature and wind speed (Uemura et al., 2008; Rahul et al., 2018; Benetti et al., 2014; Midhun et al., 2013). Therefore, it serves as a proxy for the moisture source conditions in the evaporation regions. The dxs and relative humidity are strongly coupled, which is determined by the magnitude of moisture gradient between evaporating water surface and overlying unsaturated air. In other words, lower the relative humidity

6

higher is the dxs in the overlying moisture. Wind speed regulates the turbulent vs molecular diffusion across the diffusive layer. The role of sst in governing the dxs is through the process of equilibrium fractionation, which is temperature dependent. The dxs values in water vapor samples range from 18.7‰ to -23.7‰. A relatively higher dxs values in the water vapor from ≈25°S to ≈45°S with a slight step change to lower dxs values was recorded on approaching 45°S which extends until ≈65°S. Beyond ≈ 65°S a slight increment in the vapor dxs was observed as depicted in the box-plot in Figure 4d. The very low dxs values, caused due to mixing of vapor evaporated from sea-spray under high wind speed conditions are observed during the passage of extra-tropical cyclones. The statistics of the isotopic composition of water vapor are tabulated in Table 1.

3.2   Meteorological controls on the isotopic composition of water vapor

The $\delta^{18}O_{wv}$ and $\delta^{2}H_{wv}$ are positively correlated with sst, negatively correlated with wind speed and uncorrelated with relative humidity. For all the water vapor samples, $\delta^{2}H_{wv}$ and $\delta^{18}O_{wv}$ are correlated with sst explaining ≈33% of the variance in $\delta^{18}O_{wv}$ and ≈50% of the variance in $\delta^{2}H_{wv}$. The correlation coefficient is higher if sampling from individual years is considered separately. In all cases, the slope and intercept of the regression equation between the isotopic composition of water vapor and sst is comparable with previous observations from the Southern Ocean Uemura et al. (2008). The linear regression plots are shown Figure 5 and the regression parameters (slope, intercept, standard errors and r^{2}) for $\delta^{18}O$ and $\delta^{2}H$ are listed in Table 1.(S) and Table 2.(S) respectively. The regression equations are calculated for different sample classifications, with and without the influence of Antarctic vapor mixing as evident from the back trajectories (i.e. samples collected north of 65°S) and for individual expeditions.

Figure 6 shows the regression plots of dxs in vapor with the meteorological conditions and the parameters defining the regression equations are listed in Table 2. For samples collected north of 65°S, the linear regression equation describing the relationship between dxs and relative humidity is dxs=-0.56h+46.36 (r^{2}=0.49). These slope and intercept values are similar to the earlier records, documenting the isotope variability in water vapour from the Southern Ocean (Uemura et al., 2008; Rahul et al., 2018) the Bay of Bengal (Midhun et al., 2013), the Atlantic (Benetti et al., 2014) and the Mediterranean (Gat et al., 2003). For samples collected south of 65°S the relationship becomes weaker. The strength of the dxs vs h relationship was stronger if data exclusively from the expeditions is considered separately, for the SOE IX and SOE X as dxs=-0.64h+57.4 (r^{2}=0.77) and dxs=-0.64h+48.7 (r^{2}=0.61) respectively. Collectively for both the expeditions, the dxs in vapor is positively correlated with the sst and the regression parameters are comparable with those from previous observations in the Southern Ocean and also for the Atlantic Ocean and the Bay of Bengal. For sst vs dxs, the linear regression equation for samples collected north of 65°S is given by dxs=0.70sst-4.65 (r^{2}=0.49). The dxs of water vapor samples are negatively correlated with wind speed. For samples collected north of 65°S the correlation the regression equation is given by dxs=-0.53ws+11.65 (r^{2}=0.23). Our observation is consistent with the earlier studies suggesting the dependency of water vapor d-excess on relative humidity, sst and wind speed.

4 Discussion

4.1 Craig-Gordon (CG) model evaluation

The isotopic composition of evaporation flux from the oceans is calculated using the CG models (TCG and UCG) assuming three molecular diffusivity ratios driving the kinetic fractionation and for varied contribution of turbulent vs molecular diffusion enabled transport factors. The simulated values of the isotopic composition of evaporation flux with these different models are compared with the measured isotopic values of water vapor over the ocean. The model and the constraints than best describes the observations are selected based on the model predicted and observed relationships between the dxs of water vapor and physical parameters (sst, ws and rh).

The TCG and the UCG models are run for MJ, CD and PW molecular diffusivities and for the turbulence index of the atmosphere varying from 0-1 with an increment of 0.1. Figure 7 and Figure 8 shows the comparison between the TCG and UCG modelled vapor isotopic composition ($\delta^{18}O$ and d-excess) with the observations. There are values for the turbulence index (x) of the atmosphere where model predicted $\delta^{18}O$ and d-excess overlap with the observations for both TCG and UCG models with MJ and CD molecular diffusivity ratios. However, there is a clear mismatch between the model predicted $\delta^{18}O$ and d-excess for the recommended PW molecular diffusivities in both UCG and TCG models. Another noteworthy feature of the plots is the for all the model runs a large difference is seen between the modelled and observed isotopic composition for water vapor samples collected south of $\approx 65°$S latitudes and the best match is seen for samples collected North of $\approx 65°$S. This difference is attributed to the advection and mixing of lighter Antarctic moisture to local moisture for samples collected beyond $\approx 65°$S.

To evaluate the performance of the prediction by these models and identify the parameters that best describe the observations, the slope of the dxs vs relative humidity predicted by the different model runs are compared with the observed relationships documented based on actual data on samples collected north of 65°S. Figure 1.(S) depicts the comparison between the observed and the model predicted relationships. The UCG models and the parameters that match the observed slope of the relative humidity vs d-excess relationship (-0.56 ± 0.08) are $UCG^{MJ}_{x=0.8}$, $UCG^{CD}_{x=0.6}$ and $UCG^{PW}_{x=0}$. Similarly for the TCG models $TCG^{MJ}_{x=0.6}$, $TCG^{CD}_{x=0.7}$ and $TCG^{PW}_{x=0}$ predict the slopes that are comparable with the observed value. The $\delta^{18}O$ d-excess of predicted by these models are plotted with the observations in Figure 9.

The consistency of model results and observation are best described using a linear regression equation which link model predicted d-excess and the meteorological parameters (relative humidity, sea surface temperature and wind speed). These regression plots are displayed in Figure 2.(S). The difference between the model predicted and the observed values of slopes and intercepts are shown in Figure 10. The largest difference between the observed and model predicted slopes are intercepts are for the PW molecular diffusivities for both UCG and the TCG models and therefore excluded from further discussion. For the dxs vs relative humidity relationship, $UCG^{MJ}_{x=0.8}$ and $UCG^{CD}_{x=0.6}$ show the smallest difference between the observed and modelled slopes and intercepts followed by $TCG^{MJ}_{x=0.6}$ and $TCG^{CD}_{x=0.7}$. In case of dxs vs sst relationship, 'the TCG models show the least difference between the slopes and the UCG model predicts the intercept values that are consistent with the observations. Similarly, for the and dxs vs ws relationships, the UCG and the TCG models produce the values that are predict

the slope and the intercept values with the least deviation from the observed values. The models that best describe the slope and intercept values of linear regression equation defining the d-excess vs the meteorological parameters, the root mean square error of the modelled vs observed $\delta^{18}O$ and d-excess are listed in Table 3. The ability of the models to predict the $\delta^{18}O$ and d-excess are better demonstrated by the water vapor samples which were collected north of 65°S are considered. The models predict the d-excess with a better correlation than $\delta^{18}O$ and the TCG model show a slightly higher possibility to predict the d-excess values than the UCG model.

4.2   Understanding the equilibrium/disequilibrium

The isotopic composition of water vapor over the ocean is governed by the equilibrium and kinetic processes which are defined by the meteorological condition. However, considering only these factors insufficient to explain the observed variation in the isotopic composition of vapor on top of the ocean. The process like advective mixing of transported vapor to the locally generated vapor is important and needs to be taken into consideration. Fig. 11a shows the difference between the $\delta^{18}O$ and $\delta^2 H$ isotopic composition of vapor (at equilibrium with ocean surface water) and the observed vapor isotopic composition. Kinetic fractionation can explain a part of the departure from the equilibrium state and is evaluated based on the Craig-Gordon models as described in the previous section ($E_{UCG}^{MJ,0.8}$, $E_{UCG}^{CD,0.6}$, $E_{TCG}^{MJ,0.6}$ and $E_{TCG}^{CD,0.7}$). The difference between isotopic composition of equilibrium vapor ($\delta^{18}O$ and $\delta^2 H$) and the modelled isotopic composition by the E_{UCG}, E_{TCG} is also plotted in Figure 11b-e. In order to calculate the fractional contribution of the local and advected moisture along the sampling transect, a two component mixing framework is invoked. The local end member is based on the isotopic composition of vapor predicted by the best match UCG and the TCG model predicted parameters. The calculations are done assuming the isotopic composition of the advected vapor due to westerlies similar to the earlier proposition (Uemura et al., 2008) ($\delta^2 H \approx$-109‰) in the region between 31°S to 65°S. For samples collected in the polar ocean south of 65°S, the temperature plays the role of limiting the local evaporation process and hence the large differences from the equilibrium conditions can be explained by invoking the process of mixing of Antarctic vapor which is transported to this region by the interplay of polar easterlies. The average isotopic composition of water vapor collected at Dome C site (Dec 2014-Jan) (Wei et al., 2019) ($\delta^2 H=$ -490±23‰) is chosen as representative of the advected vapor transported by the polar easterlies. It is seen that in order to explain the water vapor isotope ratio observation over the ocean south of 65°S, the contribution of lighter Antarctic vapor is expected. Fig. 12b shows the relative contribution of advected and locally generated moisture in our observation. The advected component is a prominent component of the ambient vapor on approaching higher latitudes. South of 65°S the amount of moisture present in the atmosphere is less and is largely local in origin with a small mixing of lighter Antarctic vapor. However, the contribution of which linearly increases on approaching the coastal regions.

5   Conclusions

In this study, the isotopic composition of water vapor and surface water samples collected across a latitudinal transect from Mauritius to Prydz in the Southern Ocean are described. The isotopic composition of evaporating vapor is governed by the iso-

topic composition of the water, ambient vapor isotopic composition, exchange and mixing processes at the water-air interface as well as the local meteorological conditions. These controlling parameters were considered separately or simultaneously for explaining the observation best quantifying the evaporation mechanism adopted in the Craig-Gordon models. The Traditional (Craig and Gordon, 1965) (TCG) and the Unified C-G (UCG) (Gonfiantini et al., 2018) equations were used to predict the isotopic composition of evaporation flux after incorporating different molecular diffusivity ratios at varying fractions of molecular and turbulent diffusion. $UCG_{x=0.8}^{MJ}, UCG_{x=0.6}^{CD}, TCG_{x=0.6}^{MJ}$ and $TCG_{x=0.7}^{CD}$ models predicted the slope and the intercepts of dxs vs meteorological parameters with an appreciable accuracy and consistent with the observations. The results ascertain the importance of the fraction of molecular vs turbulent fraction used to predict the isotopic composition of evaporation in the Craig-Gordon models. The relative contribution of advected and evaporated fluxes was estimated by assigning end member isotopic composition and solving in a two-component mixing framework. The approximation of the locally generated end member composition is based on $UCG_{x=0.8}^{MJ}, UCG_{x=0.6}^{CD}, TCG_{x=0.6}^{MJ}$ and $TCG_{x=0.7}^{CD}$. The advected moisture flux is assigned values based on the origin and path followed by the back trajectories. It is found that beyond 65S latitude lighter isotope values observed in the water can be explained by invoking mixing of Antarctic vapor with linearly increasing contribution towards the coast.

Author contributions

SSD and PG conceptualized the study. SSD and AS performed the sample collection and analysis. SSD wrote the paper and PG supervised the study. AK provided the resources during the expeditions.

Data Availability

The data that support the findings of this study have been uploaded as a supplementary document.

Declaration of interests

The authors declare that they have no known competing financial interests or personal relationships that could have appeared to influence the work reported in this paper.

References

Araguás-Araguás, L., Froehlich, K., and Rozanski, K.: Deuterium and oxygen-18 isotope composition of precipitation and atmospheric moisture, Hydrological Processes, 14, 1341–1355, 2000.

Benetti, M., Reverdin, G., Pierre, C., Merlivat, L., Risi, C., Steen-Larsen, H. C., and Vimeux, F.: Deuterium excess in marine water vapor: Dependency on relative humidity and surface wind speed during evaporation, Journal of Geophysical Research: Atmospheres, 119, 584–593, 2014.

Benetti, M., Aloisi, G., Reverdin, G., Risi, C., and Sèze, G.: Importance of boundary layer mixing for the isotopic composition of surface vapor over the subtropical North Atlantic Ocean, Journal of Geophysical Research: Atmospheres, 120, 2190–2209, 2015.

Benetti, M., Reverdin, G., Aloisi, G., and Sveinbjörnsdóttir, Á.: Stable isotopes in surface waters of the Atlantic Ocean: Indicators of ocean-atmosphere water fluxes and oceanic mixing processes, Journal of Geophysical Research: Oceans, 122, 4723–4742, 2017a.

Benetti, M., Steen-Larsen, H. C., Reverdin, G., Sveinbjörnsdóttir, Á. E., Aloisi, G., Berkelhammer, M. B., Bourlès, B., Bourras, D., De Coetlogon, G., Cosgrove, A., et al.: Stable isotopes in the atmospheric marine boundary layer water vapour over the Atlantic Ocean, 2012–2015, Scientific data, 4, 160 128, 2017b.

Cappa, C. D., Hendricks, M. B., DePaolo, D. J., and Cohen, R. C.: Isotopic fractionation of water during evaporation, Journal of Geophysical Research: Atmospheres, 108, 2003.

Chahine, M. T.: The hydrological cycle and its influence on climate, Nature, 359, 373, 1992.

Craig, H.: Isotopic variations in meteoric waters, Science, 133, 1702–1703, 1961.

Craig, H. and Gordon, L. I.: Deuterium and oxygen 18 variations in the ocean and the marine atmosphere, 1965.

Dansgaard, W.: Stable isotopes in precipitation, Tellus, 16, 436–468, 1964.

Draxler, R. R. and Hess, G.: An overview of the HYSPLIT_4 modelling system for trajectories, Australian meteorological magazine, 47, 295–308, 1998.

Galewsky, J., Steen-Larsen, H. C., Field, R. D., Worden, J., Risi, C., and Schneider, M.: Stable isotopes in atmospheric water vapor and applications to the hydrologic cycle, Reviews of Geophysics, 54, 809–865, 2016.

Gat, J., Klein, B., Kushnir, Y., Roether, W., Wernli, H., Yam, R., and Shemesh, A.: Isotope composition of air moisture over the Mediterranean Sea: an index of the air–sea interaction pattern, Tellus B, 55, 953–965, 2003.

Gat, J. R.: Oxygen and hydrogen isotopes in the hydrologic cycle, Annual Review of Earth and Planetary Sciences, 24, 225–262, 1996.

Gonfiantini, R., Wassenaar, L. I., Araguas-Araguas, L., and Aggarwal, P. K.: A unified Craig-Gordon isotope model of stable hydrogen and oxygen isotope fractionation during fresh or saltwater evaporation, Geochimica et Cosmochimica Acta, 235, 224–236, 2018.

Horita, J. and Wesolowski, D. J.: Liquid-vapor fractionation of oxygen and hydrogen isotopes of water from the freezing to the critical temperature, Geochimica et Cosmochimica Acta, 58, 3425–3437, 1994.

Kanamitsu, M., Ebisuzaki, W., Woollen, J., Yang, S.-K., Hnilo, J., Fiorino, M., and Potter, G.: Ncep–doe amip-ii reanalysis (r-2), Bulletin of the American Meteorological Society, 83, 1631–1643, 2002.

Korzoun, V. and Sokolov, A.: World water balance and water resources of the earth, Water Development, Supply and Management (UK)(USA)(Canada)(Australia)(France)(Germany, FR), 1978.

Merlivat, L.: Molecular diffusivities of H 2 16 O, HD 16 O, and H 2 18 O in gases, The Journal of Chemical Physics, 69, 2864–2871, 1978.

Midhun, M., Lekshmy, P., and Ramesh, R.: Hydrogen and oxygen isotopic compositions of water vapor over the Bay of Bengal during monsoon, Geophysical Research Letters, 40, 6324–6328, 2013.

320   Noone, D. and Sturm, C.: Comprehensive dynamical models of global and regional water isotope distributions, in: Isoscapes, pp. 195–219, Springer, 2010.

Oki, T. and Kanae, S.: Global hydrological cycles and world water resources, science, 313, 1068–1072, 2006.

Pfahl, S. and Wernli, H.: Lagrangian simulations of stable isotopes in water vapor: An evaluation of nonequilibrium fractionation in the Craig-Gordon model, Journal of Geophysical Research: Atmospheres, 114, 2009.

325   Prasanna, K., Ghosh, P., Bhattacharya, S., Rahul, P., Yoshimura, K., and Anilkumar, N.: Moisture rainout fraction over the Indian Ocean during austral summer based on 18O/16O ratios of surface seawater, rainwater at latitude range of 10 N-60 S., Journal of Earth System Science, 127, 2018.

Rahul, P., Prasanna, K., Ghosh, P., Anilkumar, N., and Yoshimura, K.: Stable isotopes in water vapor and rainwater over Indian sector of Southern Ocean and estimation of fraction of recycled moisture, Scientific reports, 8, 2018.

330   Schmidt, G., Bigg, G., and Rohling, E.: Global seawater oxygen-18 database–v1. 21, Online at http://data. giss. nasa. gov/o18data, online at http://data. giss. nasa. gov/o18data, 1999.

Shiklomanov, I. A.: World water resources: a new appraisal and assessment for the 21st century: a summary of the monograph World water resources, Unesco, 1998.

Stein, A., Draxler, R., Rolph, G., Stunder, B., Cohen, M., and Ngan, F.: NOAA's HYSPLIT atmospheric transport and dispersion modeling

335   system, Bulletin of the American Meteorological Society, 96, 2059–2077, 2015.

Trenberth, K. E.: Atmospheric moisture residence times and cycling: Implications for rainfall rates and climate change, Climatic change, 39, 667–694, 1998.

Uemura, R., Matsui, Y., Yoshimura, K., Motoyama, H., and Yoshida, N.: Evidence of deuterium excess in water vapor as an indicator of ocean surface conditions, Journal of Geophysical Research: Atmospheres, 113, 2008.

340   Van Der Ent, R. J. and Tuinenburg, O. A.: The residence time of water in the atmosphere revisited, Hydrology and Earth System Sciences, 21, 779–790, 2017.

Wei, Z., Lee, X., Aemisegger, F., Benetti, M., Berkelhammer, M., Casado, M., Caylor, K., Christner, E., Dyroff, C., García, O., et al.: A global database of water vapor isotopes measured with high temporal resolution infrared laser spectroscopy, Scientific data, 6, 180 302, 2019.

345   Yoshimura, K.: Stable water isotopes in climatology, meteorology, and hydrology: A review, Journal of the Meteorological Society of Japan. Ser. II, 93, 513–533, 2015.
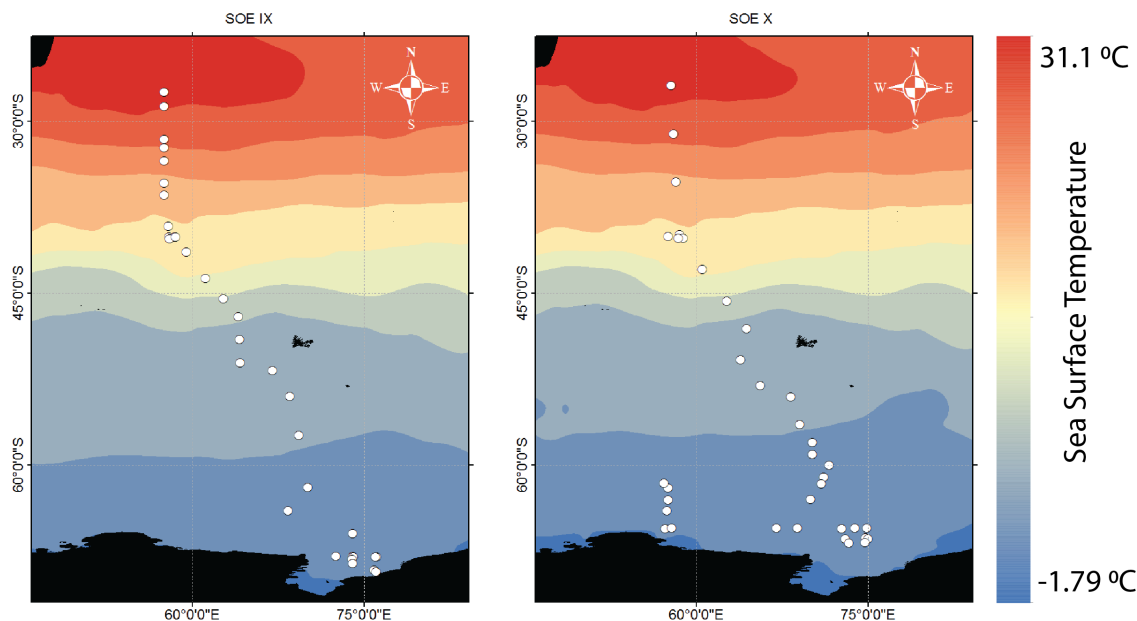
Figure 1. The water vapor sampling location during the two expedition shown as open circles overlain on the map of mean monthly sea surface temperature during the two expeditions. The sea surface temperature data is from Reanalysis dataset Kanamitsu et al. (2002)

Table 1. Descriptive statistics of the water vapor isotopic composition

	$\delta^{18}O(‰)$	$\delta^2H(‰)$	**d-excess**$(‰)$
	SOE IX Water Vapor(n=34)		
Max	-10.86	-80.79	18.65
Min	-27.47	-221.38	-8.37
Mean(Stdev)	-16.96(±5.25)	-130.35(±44.43)	5.35(±8.06)
	SOE X Water Vapor(n=37)		
Max	-11.46	-88.03	14.54
Min	-21.18	-163.28	-23.71
Mean(Stdev)	-15.77(±2.53)	-126.07(±20.23)	0.08(±8.46)
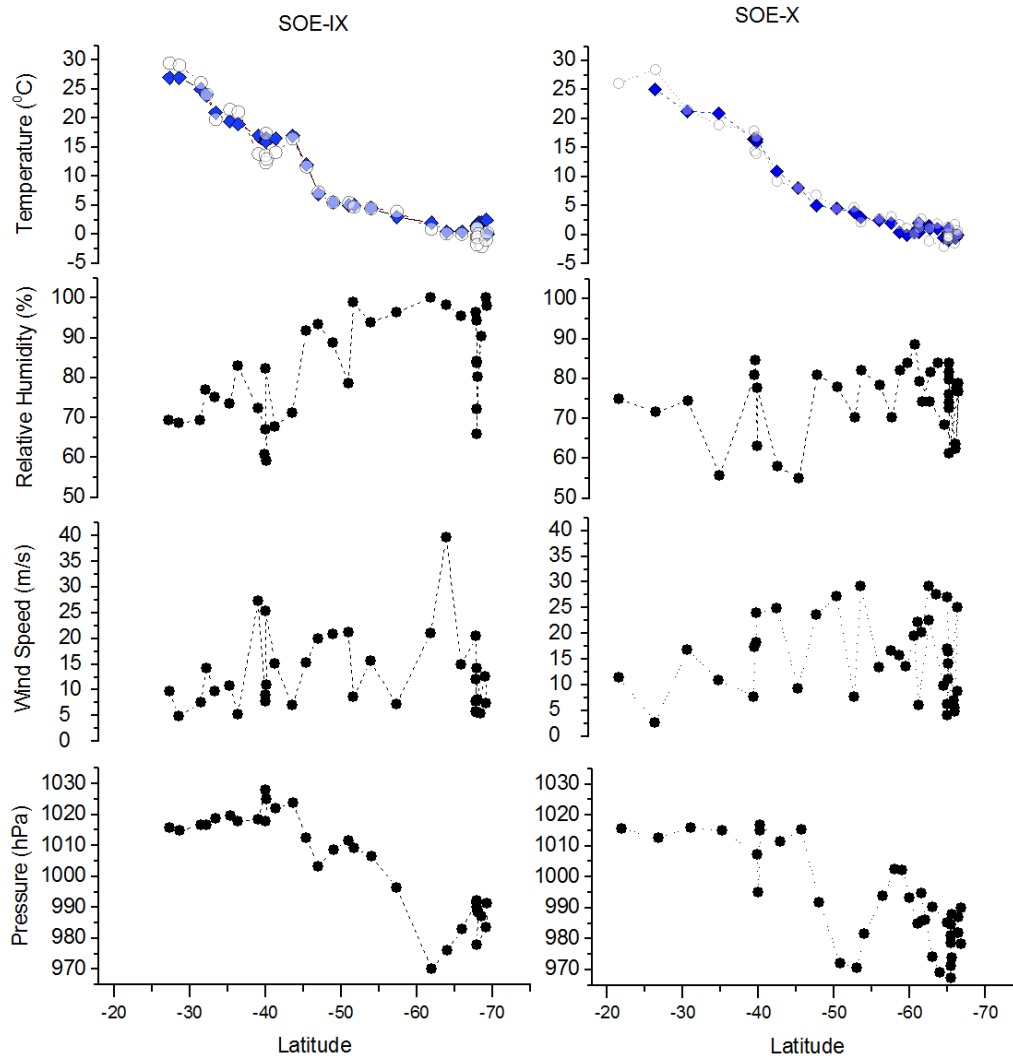
Figure 2. Latitudinal variability of measured meteorological parameters, temperature, relative humidity, wind speed and atmospheric pressure. Filled blue diamonds and open circles in the temperature plot represent the sea surface temperature and air temperature respectively.
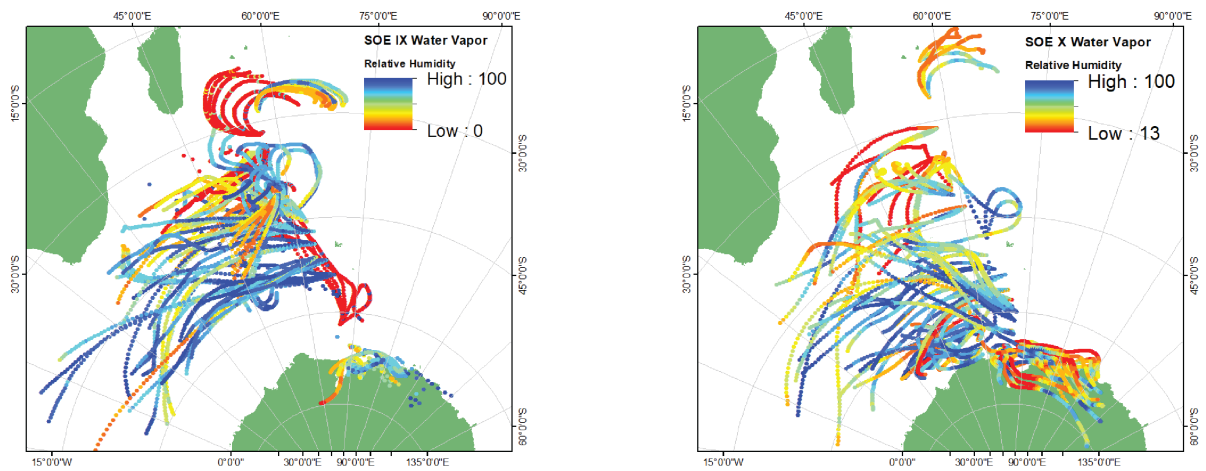
Figure 3. 72 hours back trajectories calculated using HYSPLIT with Reanalysis data as forcing. The trajectories shown are for three heights surface, 500m and 1500m above the mean sea level and the colors depict the variation of relative humidity along the trajectories.
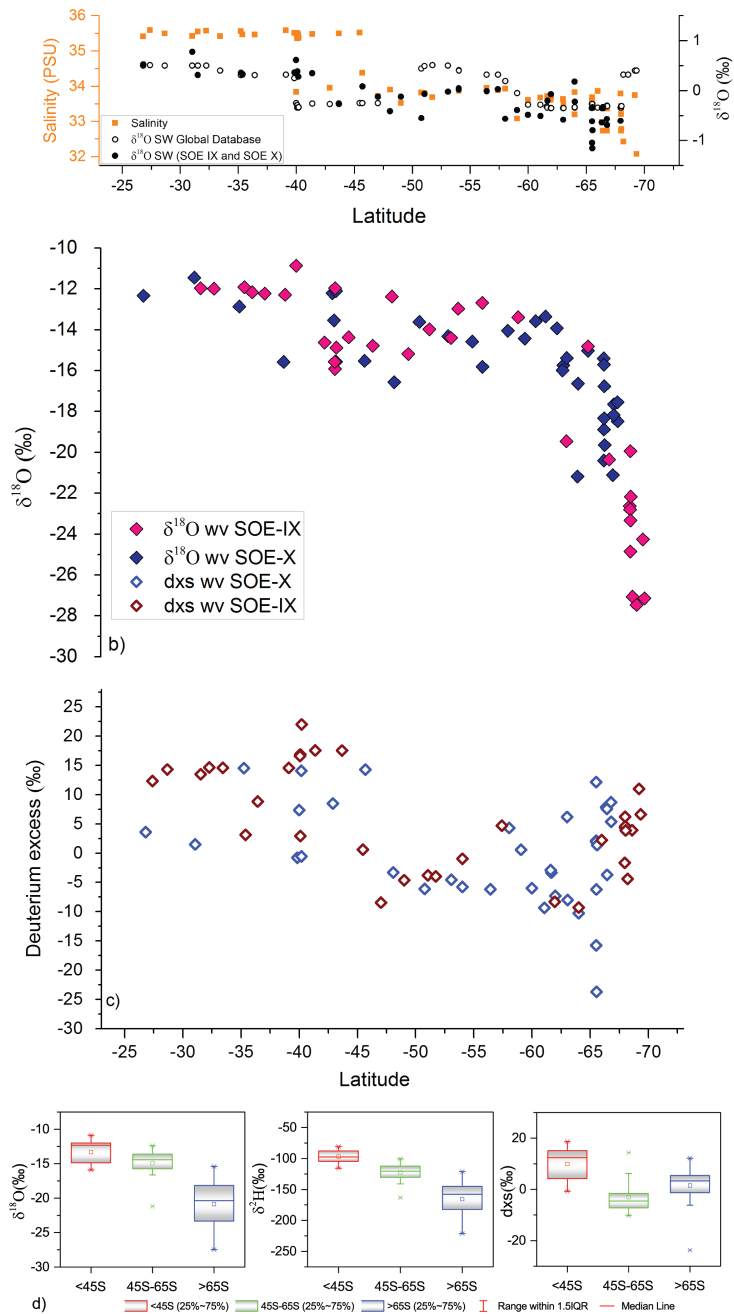
Figure 4. a) Measured $\delta^{18}O_{SW}$ as black filled circled and values of surface water isotopic composition extracted from the global sea water $\delta^{18}O_{SW}$ database along the latitudinal transect (open black circles). Also plotted as orange filled squares are the salinity values along the transect b) Pink and purple filled diamonds depict the $\delta^{18}O_{WV}$ of water vapor samples collected during the SOE-IX and SOE-X respectively at height of $\approx$ 15m above the water surface. c) latitudinal variation of dxs in water vapor samples shown as open red and purple diamonds for SOE-IX and SOE-X respectively, d) variation of $\delta^{18}O$, δ^2H and dxs along the transect as box plots grouped by latitudes based on the HYSPLIT back trajectories.
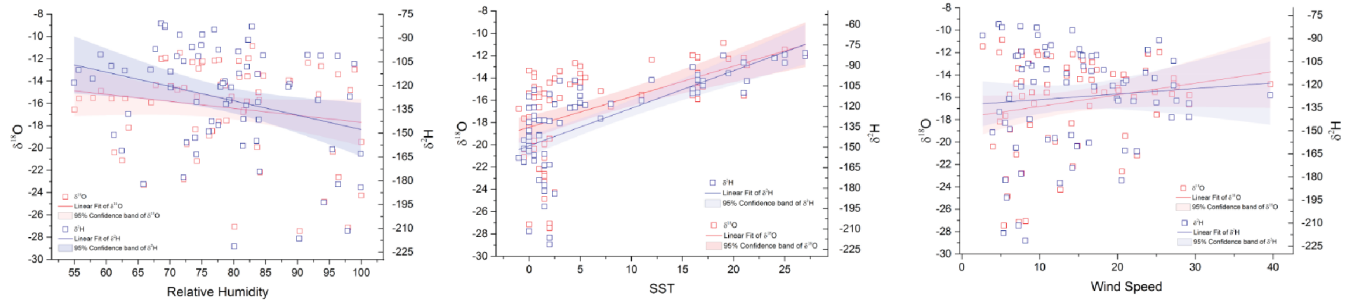
Figure 5. Linear regression for isotopic composition of water vapor and physical parameters(sea surface temperature, relative humidity and wind speed). Hollow red and blue squares represent the $\delta^{18}O$ and $\delta^{2}H$ respectively and the shaded areas depict the 95% confidence bands. The linear regression lines are shown as blue and red for $\delta^{2}H$ and $\delta^{18}O$ respectively. The slope and intercept of the linear regression equations along with data from Uemura et al. (2008) are listed in Table 1.(S) and Table 2.(S)
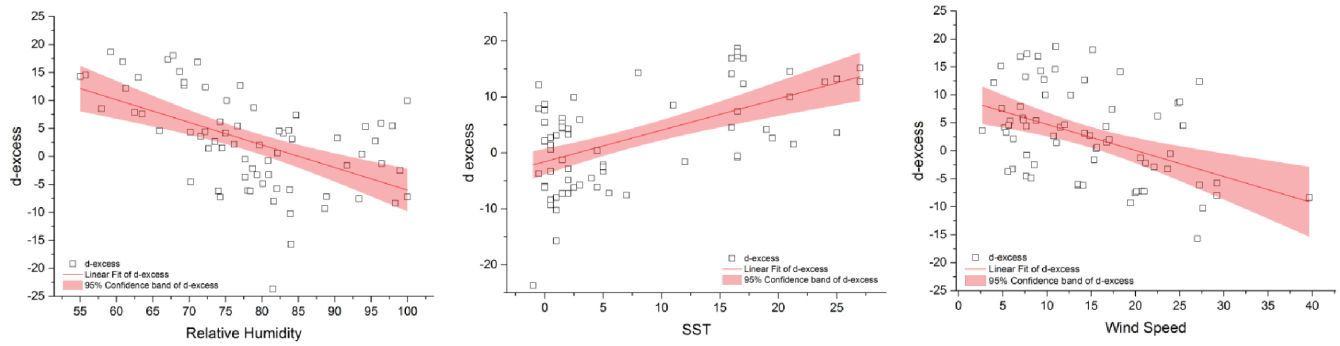

Figure 6. Regression plots for d-excess (hollow black squares) in water vapor and the meteorological conditions (relative humidity, sea surface temperature and wind speed). The shaded region depicts the 95% confidence bands of d-excess. The slope and intercept of the regression equations along with data from Uemura et al. (2008) are listed in Table 2
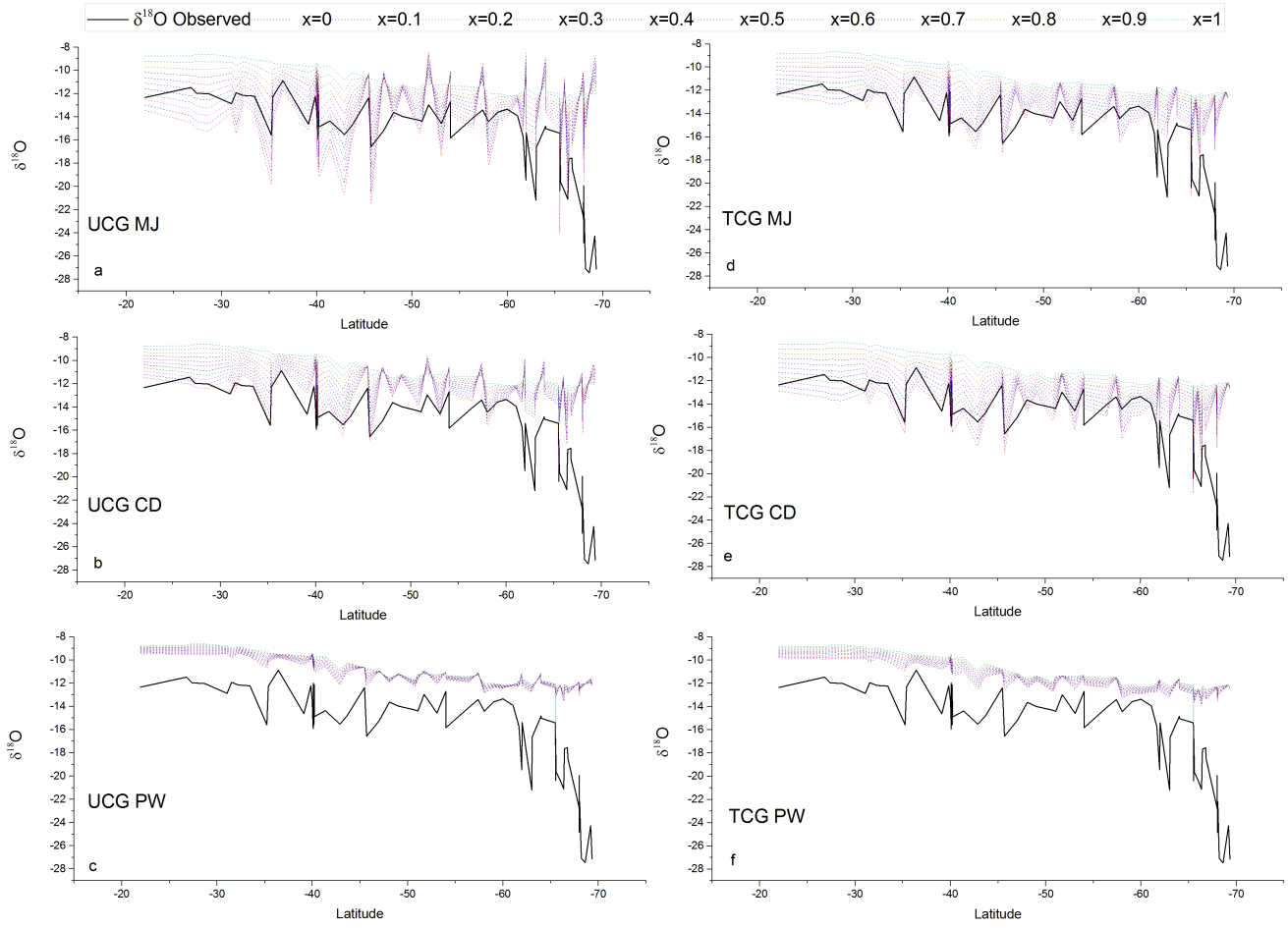
Figure 7. Comparison between the latitudinal distribution of the measured water vapor $\delta^{18}O$ (black lines) and that predicted by the TCG and UCG models for different molecular diffusivity ratios and turbulence indices, shown as colored lines.

Figure 8. Comparison between the latitudinal distribution of the measured d-excess in water vapor (black lines) and that predicted by the TCG and UCG models for different molecular diffusivity ratios and turbulence indices shown as colored lines
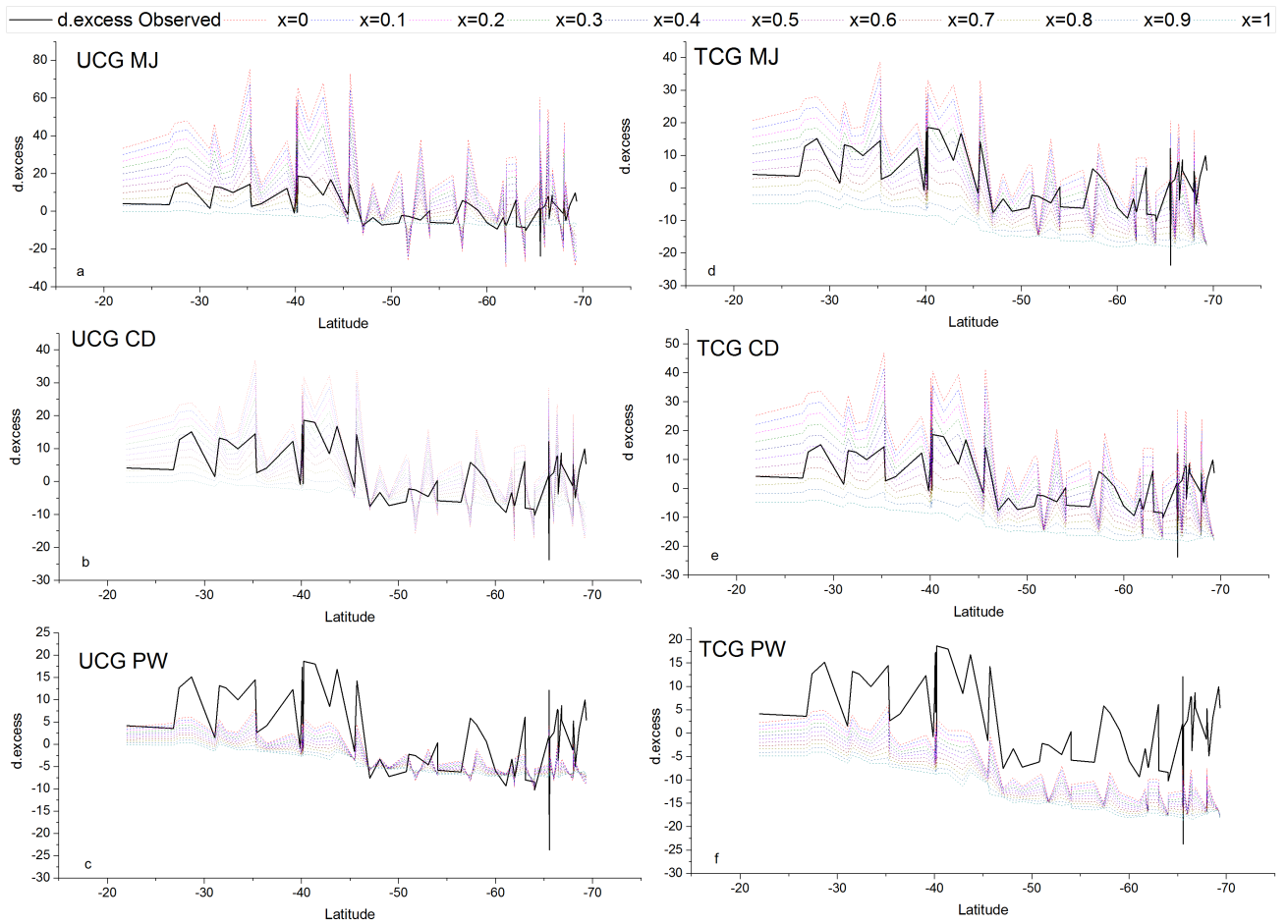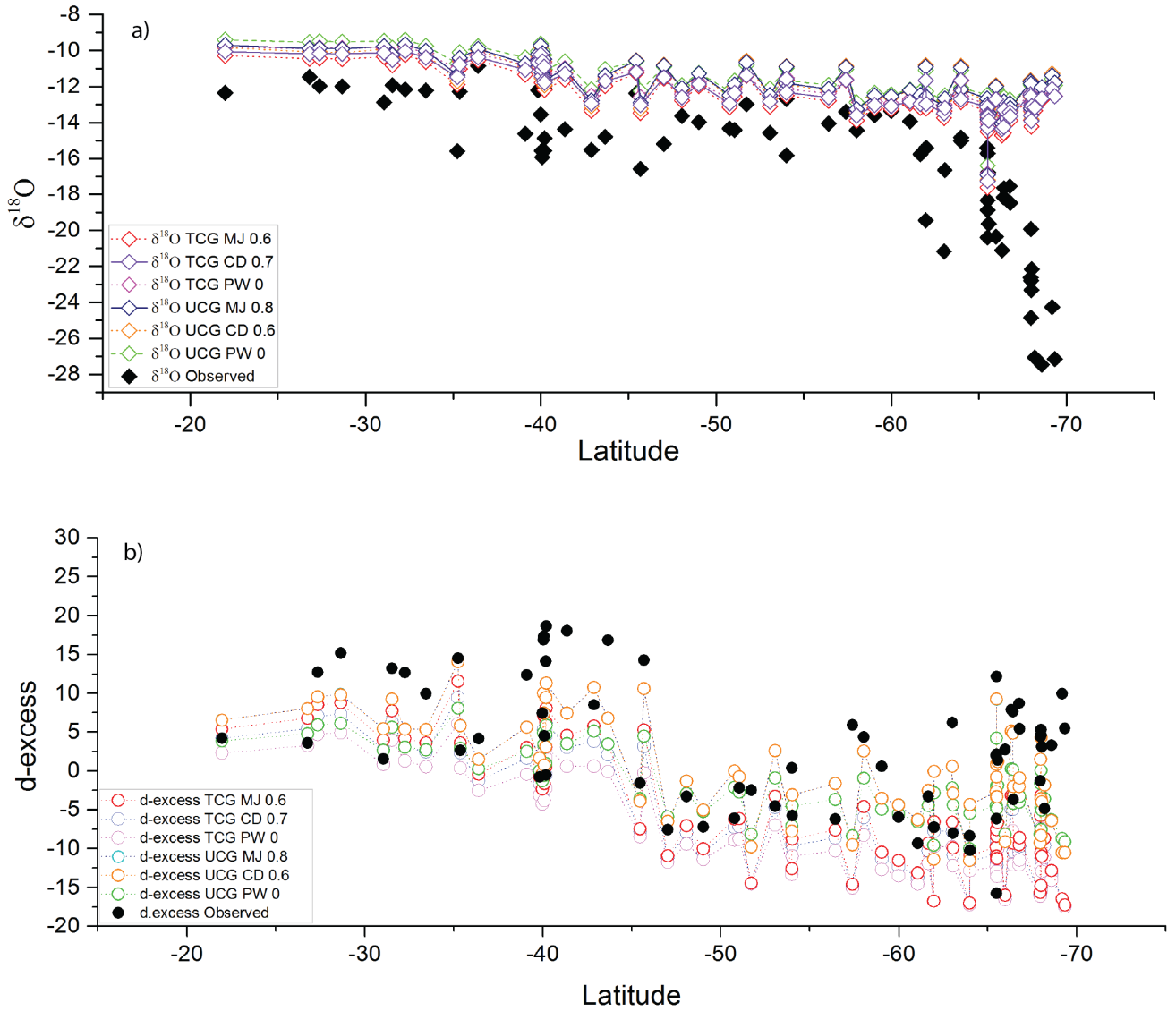
Figure 9. Latitudinal variation of the observed $\delta^{18}O$ (a) as filled black diamonds and d-excess (b) as filled black circles and the modelled values (colored open diamonds and circles) for the model runs where the observed slope is comparable to the modelled slope. The statistical parameters analysis of the observed and modelled regression are listed in Table 3.
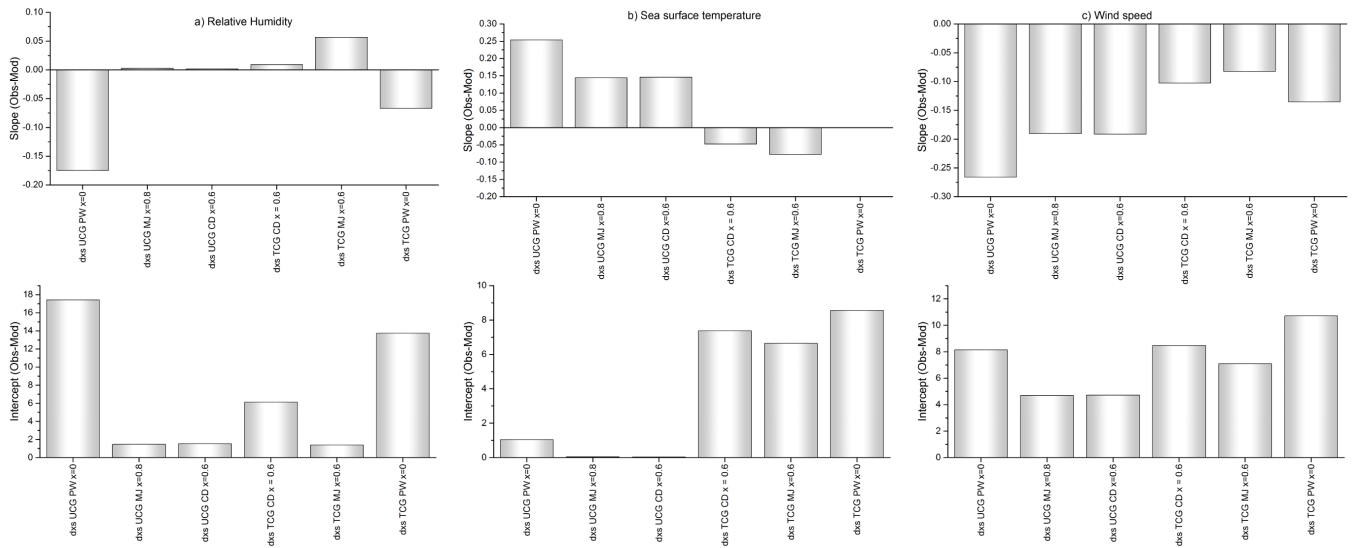
Figure 10. Differences between observed and predicted slopes and intercepts of the relationships between d-excess vs relative humidity, sea surface temperature and wind speed.
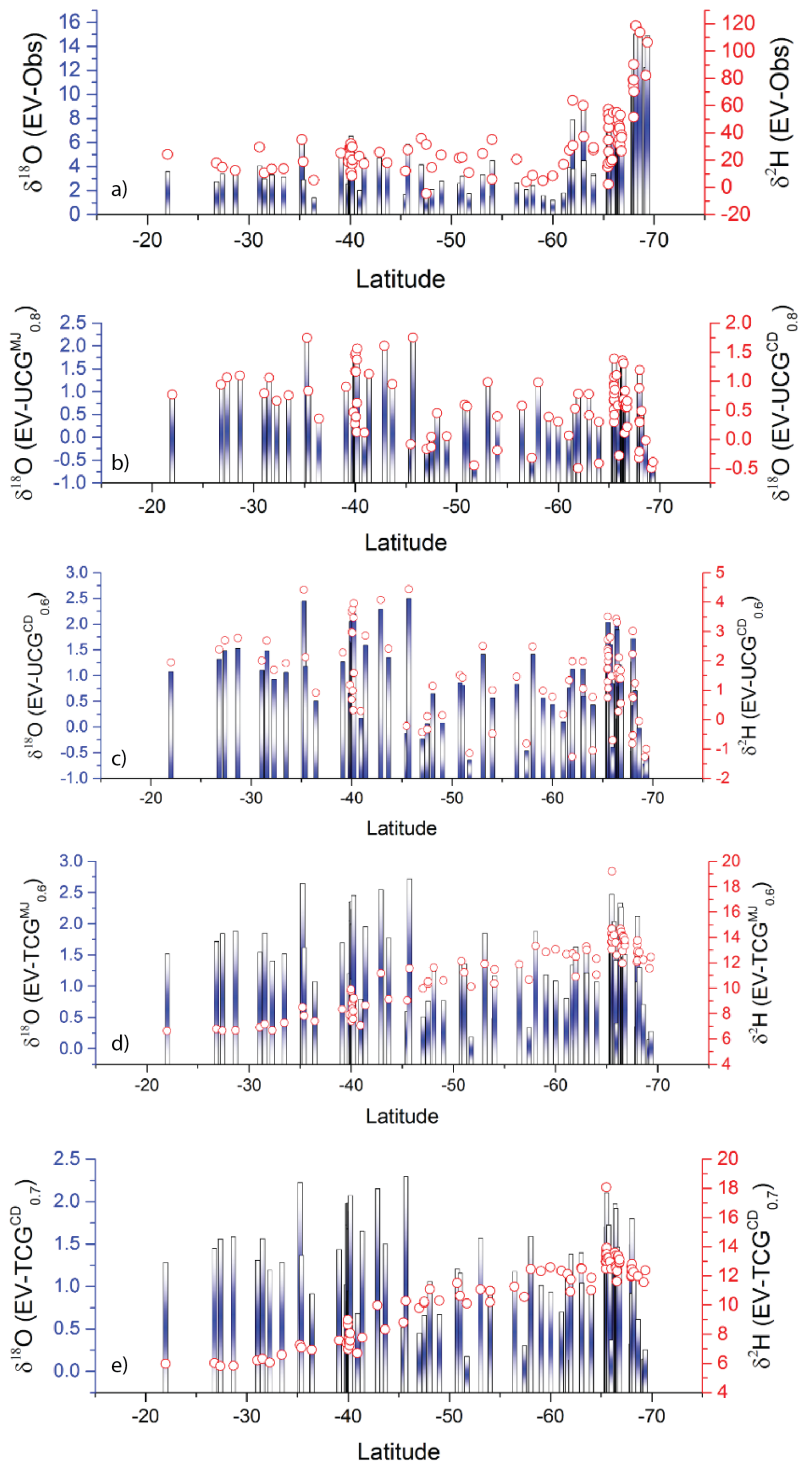
Figure 11. a) the difference between the $\delta^{18}O$ (blue columns) and δ^2H (red open circles) of equilibrium vapor and observed water vapor isotopic composition. b-e) shows difference between the $\delta^{18}O$ and δ^2H equilibrium vapor and that predicted by the best fit model runs.

Figure 12. a) Fraction of advected vapor that explains the water vapor isotopic composition for the best fit model runs. Red and blue colors depict the different end member compositions used for calculations.

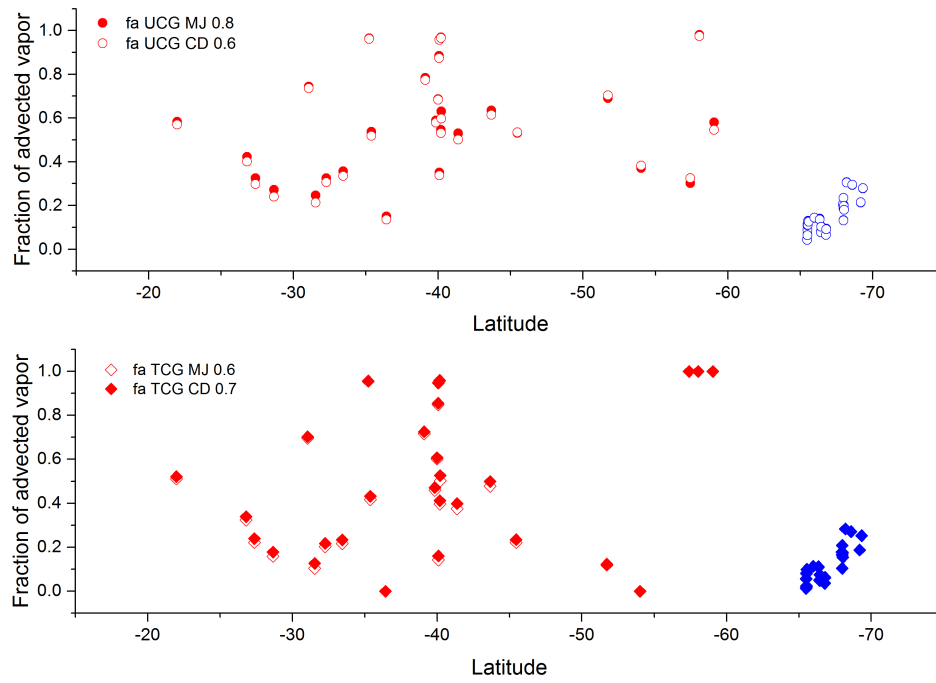**Table 2.** Slope, intercept and r^2 of the linear regression equations between meteorological parameters (relative humidity, sea surface temperature and winds speed) and d-excess for different sample classifications. Also listed are the regression parameters for the data from Uemura et al. (2008)

Met. vs d-excess	Classification	Intercept		Slope		Statistics
		Value	Standard Error	Value	Standard Error	R-Square(COD)
Relative Humidity	ALL	34.31	6.23	-0.40	0.08	0.28
	ALL North of 65S	46.36	6.57	-0.56	0.08	0.49
	ALL South of 65S	8.35	12.49	-0.08	0.15	0.01
	SOE IX North of 65S	57.40	6.15	-0.64	0.08	0.77
	SOE X North of 65S	48.66	8.28	-0.64	0.11	0.61
	ALL SOE X	53.37	8.93	-0.71	0.12	0.51
	ALL SOE IX	42.72	6.54	-0.45	0.08	0.51
	Uemura All	54.12	4.27	-0.58	0.05	0.66
	Uemura North of 65S	55.71	5.82	-0.61	0.08	0.62
Sea Surface Temperature	ALL	-1.58	1.15	0.56	0.10	0.31
	ALL North of 65S	-4.83	1.46	0.74	0.11	0.52
	ALL South of 65S	0.59	2.06	1.50	1.81	0.03
	SOE IX North of 65S	-5.54	2.63	0.84	0.16	0.56
	SOE X North of 65S	-4.18	1.76	0.56	0.16	0.35
	ALL SOE X	-2.19	1.62	0.43	0.18	0.14
	ALL SOE IX	-0.36	1.60	0.58	0.12	0.42
	Uemura All	4.13	0.98	0.79	0.12	0.43
	Uemura North of 65S	3.43	1.35	0.85	0.13	0.53
Wind Speed	ALL	9.40	1.97	-0.47	0.12	0.18
	ALL North of 65S	11.68	2.54	-0.53	0.14	0.24
	ALL South of 65S	7.74	3.22	-0.55	0.25	0.19
	SOE IX North of 65S	15.16	3.35	-0.61	0.20	0.31
	SOE X North of 65S	5.93	3.67	-0.33	0.19	0.11
	ALL SOE X	6.08	2.96	-0.38	0.17	0.13
	ALL SOE IX	11.58	2.51	-0.47	0.17	0.20

Table 3. Slope, intercept and r^2 of the linear regression equations between observed and modelled $\delta^{18}O$ and d-excess for the best fit models for samples collected north of 65S

Observed vs Modelled		Intercept		Slope		Statistics	
		Value	Standard Error	Value	Standard Error	Adj. R-Square	Root-MSE (SD)
$\delta^{18}O$ All	UCG MJ 0.8	-8.88	0.57	0.18	0.03	0.28	1.15
	UCG CD 0.6	-9.06	0.59	0.17	0.04	0.26	1.20
	TCG MJ 0.6	-9.42	0.57	0.19	0.03	0.30	1.15
	TCG CD 0.7	-9.15	0.55	0.19	0.03	0.32	1.12
$\delta^{18}O$ North of 65S	UCG MJ 0.8	-6.45	0.89	0.34	0.06	0.38	0.84
	UCG CD 0.6	-6.50	0.91	0.34	0.06	0.38	0.86
	TCG MJ 0.6	-7.02	0.91	0.34	0.06	0.38	0.86
	TCG CD 0.7	-6.89	0.91	0.34	0.06	0.37	0.86
d-excess All	UCG MJ 0.8	-0.94	0.64	0.47	0.07	0.39	5.08
	UCG CD 0.6	-0.94	0.64	0.47	0.07	0.39	5.07
	TCG MJ 0.6	-6.46	0.75	0.58	0.08	0.41	6.00
	TCG CD 0.7	-7.39	0.71	0.55	0.08	0.41	5.66
d-excess North of 65S	UCG MJ 0.8	-0.35	0.63	0.60	0.07	0.63	4.07
	UCG CD 0.6	-0.36	0.63	0.60	0.07	0.63	4.06
	TCG MJ 0.6	-4.93	0.72	0.74	0.08	0.67	4.67
	TCG CD 0.7	-5.85	0.68	0.70	0.07	0.66	4.41